CRYSTAL GROWTH & DESIGN
2008
VOL. 8, NO. 3
1023–1030

Investigations on Iron Sulfide Nanosheets Prepared via a Single-Source Precursor Approach

Wei Han and Mingyuan Gao*

Key Laboratory of Colloid, Interface Science and Chemical Thermodynamics, Institute of Chemistry, Chinese Academy of Sciences, Zhong Guan Cun, Bei Yi Jie 2, Beijing 100080, China

Received October 31, 2007; Revised Manuscript Received January 4, 2008

ABSTRACT: Two-dimensional (2D) magnetic pyrrhotite (Fe_7S_8) and greigite (Fe_3S_4) nanosheets were synthesized by pyrolyzing, respectively, single-source precursors such as $Fe(Ddtc)_2(Phen)$ (Phen = 1,10-phenanthroline; Ddtc = diethyldithiocarbamate) and $Fe(Ddtc)_3$ in oleylamine. Under optimized reaction temperature of 280 °C, both monoclinic Fe_7S_8 and cubic Fe_3S_4 obtained presented hexagonal sheet structure with sizes of 500–800 nm and 100–500 nm, respectively. AFM measurements revealed that both of these two types of nanosheets had a nearly identical thickness of 50 nm. Further XRD measurements revealed that the reaction temperature played a critical role in determining the crystalline structure as well as the chemical composition of the resultant nanosheets. In the reaction temperature range of 240−320 °C, a higher reaction temperature generally favored the transformations of monoclinic Fe_7S_8 to hexagonal FeS, and cubic Fe_3S_4 to hexagonal Fe_7S_8, respectively. The magnetic properties of the resultant nanosheets were accordingly altered against the reaction temperature. Further experimental results obtained by combining different types of solvents suggested that oleylamine was necessary for the formation of hexagonal Fe_7S_8 nanosheets. In contrast, it only helped prevent the hexagonal Fe_3S_4nanosheets from agglomeration. It was also found that both pyrrhotite (Fe_7S_8) and greigite (Fe_3S_4) nanosheets were metastable under ambient conditions. Systematic XPS measurements were carried out to investigate the air stabilities of the resultant nanosheets.

Introduction

In the past decade, magnetic nanomaterials have attracted more and more attention because of their extensive applications in ultrahigh-density magnetic storage,[1] biological assay and separation,[2,3] clinical detection,[4] diagnosis, and treatment.[5–7] Among the magnetic nanomaterials, iron oxides such as magnetite (Fe_3O_4) and maghemite (γ-Fe_2O_3) nanocrystals have intensively been investigated for the above-mentioned applications. In contrast, nanosized iron sulfides as important members of magnetic iron chalcogenide have not received enough attention yet.

In nature, there exist various types of iron sulfides with Fe:S ratio ranging from 0.5 to 1.05, correspondent to FeS_2 (marcasite, pyrite), Fe_3S_4 (greigite), $Fe_{1-x}S$ (pyrrhotite, $x < 0-0.125$; troilite, $x = 0$; mackinawite, $x = -0.05$).[8] In general, iron sulfide minerals present interesting and unique magnetic and electrical properties which are strongly related to the stoichiometric ratio between Fe and S as well as their crystalline structure.[8–10] Among the natural iron sulfide minerals, pyrrhotite and greigite are ferrimagnetic; pyrite and marcasite are diamagnetic; mackinawite is paramagnetic; and troilite is antiferromagnetic.[8,11,12]

Up until now, there have been only a limited number of low-dimensional iron sulfide materials reported in the literature. For example, pyrrhotite ($Fe_{1-x}S$, $x = 0.12$ and 0.09) nanowires with a diameter around 100 nm were prepared by pyrolyzing one-dimensional organic–inorganic hybrid precusor.[13] The resultant nanowire was of a multicrystalline structure. By hydrothermal method, diamagnetic FeS_2 (marcasite) and ferrimagnetic Fe_3S_4 rods with a diameter up to micrometers were synthesized with the aid of external magnetic fields.[14] Also by hydrothermal method, the preparation of submicrometer-sized FeS_2 (pyrite) cubes was reported using $Fe(Ddtc)_3$ (Ddtc = diethyldithiocarbamate) as a single-source precursor.[15] By a high-temperature approach, Fe_7S_8 (pyrrhotite) with highly interconnected structures of rods and sheets were obtained in KI flux using sulfur and iron powders as the starting materials.[16] Recently, by directly mixing the ferrous salt and sodium sulfide in aqueous solution in the presence of dendrimer, antiferromagnetic FeS nanoparticles were synthesized for environmental remediation applications.[17]

From the aforementioned examples, it can be concluded that the synthesis of nanosized iron sulfides with well-defined structures are far away from mature in comparison with their counterparts, iron oxides. The challenges can be summarized as follows. First, the stoichiometry for iron sulfides is much more complicated than iron oxides due to the coexistences of strongly reducible ferric ion and oxidizable sulfide ion. Second, ferric ion has a very strong affinity to oxygen, therefore, it is difficult to exclude iron oxide or iron hydroxide impurities from the resultant materials. Last but not least, the reaction temperature needs to be well-controlled because of the complicated phase diagram of iron sulfides.

In general, the morphological control is one of the most important issues concerning the low dimensional materials, especially nanomaterials.[18] Small chelating molecules have been demonstrated to be effective in controlling the morphologies of iron oxides, ranging from spherical particles,[19] polyhedron,[20,21] rods,[22,23] dendritic[24] to two-dimensional sheets[25] by balancing the growth rates of different crystallographic facets. Therefore, small molecular weight ligands may also be useful for controlling the morphology of iron sulfide nanomaterials. Regarding the composition control, the exclusions of any reactive oxygen-containing moiety from both surface capping agents and precursors is necessary for excluding unwanted impurities of iron oxides from the products. Therefore, in the current investigations, we chose oleylamine as a coordinating solvent in the syntheses of iron sulfide nanoparticles. In addition, two iron complexes, i.e., $Fe(Ddtc)_2(Phen)$ (Phen = 1,10-phenanthroline) and $Fe(Ddtc)_3$, were carefully chosen as the single-source precursor, because both iron and sulfur elements exist

* To whom correspondence should be addressed. E-mail: gaomy@iccas.ac.cn. Fax: 0086 10 8261 3214.

10.1021/cg701075u CCC: $40.75
Published on Web 02/09/2008

in these two complexes. Consequently, there was no oxygen element presented in the reaction system. By pyrolyzing $Fe(Ddtc)_2(Phen)$ and $Fe(Ddtc)_3$ directly in oleylamine, we obtained hexagonally shaped nanosheets of ferrimagnetic pyrrhotite (Fe_7S_8) and greigite (Fe_3S_4), respectively. Systematic experiments were carried out for investigating effects of reaction temperature, reaction time, and nature of ligands on the crystalline structures, magnetic properties, and morphologies of the final products. In addition, the air-stabilities of Fe_7S_8 and Fe_3S_4 nanosheets were also investigated by X-ray photoelectron spectroscopy through composition analysis.

Experimental Section

Chemicals. Ferrous sulfate heptahydrated ($FeSO_4 \cdot 7H_2O$, ≥99%), ferric chloride hexahydrated ($FeCl_3 \cdot 6H_2O$, ≥99%), sodium diethyldithiocarbamate trihydrate, ($Na(Ddtc) \cdot 3H_2O$, ≥99%), and 1,10-phenanthroline trihydrate ($(Phen) \cdot 3H_2O$, ≥ 99%) were purchased from Beijing Chemical Company and used as received. Oleylamine (≥70%) and 1-octadecene (≥95%) were used as received from Fluka. Phenylamine was commercially available product and used after purification by reduced pressure distillation. Other solvents such as ethanol, acetone, and chloroform were analytical grade and used as received.

Synthesis of $Fe(Ddtc)_2(Phen)$. $Fe(Ddtc)_2(Phen)$ was synthesized according to a literature method.[27] Typically, a hot aqueous solution of $(Phen) \cdot 3H_2O$, prepared by dissolving 5 mmol $(Phen) \cdot 3H_2O$ in 40 mL of boiling water, was introduced under vigorous stirring into 20 mL aqueous solution of $FeSO_4 \cdot 7H_2O$ (5 mmol). The reaction between Phen and ferrous ions turned the color of the reaction mixture to dark red. Approximately 10 min later, 20 mL of an aqueous solution of $Na(Ddtc) \cdot 3H_2O$ (10 mmol) was dripped dropwise into the above-mentioned dark red solution. Upon further reaction, the color of the aqueous mixture changed to turbid brown. After approximately 2 h, the resultant brown precipitate was collected by vacuum filtration, followed by three times washing with water. The brown powder obtained was stored in a vacuum desiccator at room temperature until water was completely eliminated.

Synthesis of $Fe(Ddtc)_3$. $Fe(Ddtc)_3$ was synthesized in a quite similar way except that Phen was absent in the reaction system.[15] In brief, 20 mL aqueous solution of $Na(Ddtc) \cdot 3H_2O$ (15 mmol) was mixed with 40 mL aqueous solution of $FeCl_3 \cdot 6H_2O$ (5 mmol) under vigorous stirring. The reaction led to a black precipitate that was collected by vacuum filtration and dried at room temperature for further characterization and reaction.

Synthesis of Iron Sulfide Nanosheets. Iron sulfide nanocrystals were prepared by pyrolyzing the aforementioned precursors in oleylamine. Typically, 0.78 mmol of iron complex was first dissolved into 20 mL of oleylamine, and then the resultant solution was purged by nitrogen gas for 30 min. After that, it was quickly heated up to 90 °C and maintained at this temperature for 10 min, followed by a further increase in the reaction temperature to a desired point. After the reaction was completed, the resultant suspension was subjected to centrifugation. The black precipitates obtained were washed in sequence by ethanol and acetone, respectively, and then redispersed in chloroform for further characterizations.

To further explore the ligand effects on the hexagonally shaped Fe_7S_8 or Fe_3S_4 nanosheets, three additional reactions were designed by using different types of coordinating solvents, noncoordinating solvent (octadecene), and mixtures of them. For example, the first solvent system was pure octadecene; the second one was a mixture of octadecene and oleylamine (5:1); and the third one was a mixture of octadecene and phenylamine (5:1). Except for the solvent system, all the other synthetic parameters including postprocessing procedures were exactly the same as those for Fe_7S_8 and Fe_3S_4 synthesized in pure oleylamine.

Characterizations. Transmission electron microscopy (TEM) images and selected area electron diffraction (SAED) patterns were recorded on a JEM-100CXII electron microscope operating at an acceleration voltage of 100 kV. The morphologies of the iron sulfide nanoparticles were investigated by atomic force microscopy (AFM) using Digital Instruments Nanoscope IIIa Multimode System (Santa Barbara, CA). Powder X-ray diffraction (XRD) was taken with the help of a Regaku D/Max-2500 diffractometer under Cu $K\alpha_1$ radiation ($\lambda = 1.54056$ Å).

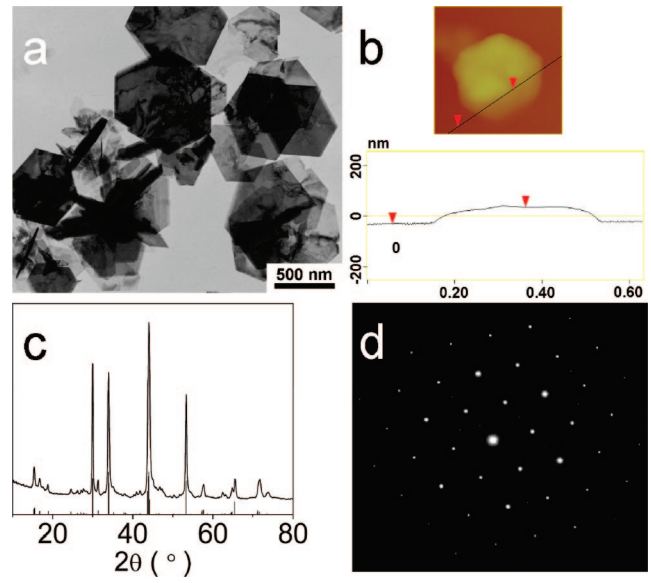

Figure 1. (a) TEM image of Fe_7S_8 nanosheets prepared at 280 °C by pyrolyzing $Fe(Ddtc)_2(Phen)$ in oleylamine; (b) AFM image and the corresponding height profile of a single nanosheet; (c) XRD pattern of the nanosheets shown in panel a. The standard diffraction lines of bulk monoclinic Fe_7S_8 (JCPDS card 29–0723) are shown at bottom for comparison; (d) SAED pattern of a single nanosheet.

Fourier transform infrared spectroscopy (FTIR) spectra were taken on a Bruker EQUINOX55 FTIR spectrometer. Magnetic measurements were carried out on a vibrating sample magnetometer (VSM JDM-13, China). X-ray photoelectron spectroscopy (XPS) measurements were performed on a VG ESCALAB 220i-XL spectrometer. All binding energies for different elements were calibrated with respect to C1s line at 284.8 eV from the contaminant carbon. A combination of a shirley-type background and a linear-type background was used for curve-fitting.

Results

The precursors of $Fe(Ddtc)_2(Phen)$ and $Fe(Ddtc)_3$ were carefully chosen and synthesized according to reference methods.[15,26] Their chemical structures were characterized and confirmed by FTIR. Detailed results are provided in the Supporting Information. Briefly, the vibrational bands of $-C-N-$ (1490 cm^{-1}) and $-C-S-$ (997 cm^{-1}) from the Ddtc moiety, and the skeleton vibrational bands of benzene ring (1622 and 1573 cm^{-1}) from the Phen moiety in $Fe(Ddtc)_2(Phen)$ shift to high energy side by 13, 10, 35, and 65 cm^{-1}, respectively, in comparison with Ddtc and Phen. Similar shifts also appear in the spectrum of $Fe(Ddtc)_3$ complex. All these variations strongly indicate that both Ddtc and Phen have coordinated with ferrous ion and ferric ion forming the target complexes, $Fe(Ddtc)_2(Phen)$ and $Fe(Ddtc)_3$, respectively.[27]

The products obtained by pyrolyzing the precursors in pure oleylamine were first analyzed by TEM. Figure 1a presents TEM results on an iron sulfide sample obtained using $Fe(Ddtc)_2(Phen)$ as precursor. The reaction temperature was 280 °C and the reaction time was 5 min. The resultant iron sulfide particles present a hexagonal sheet structure with an opposite side distance of 550–800 nm. The thickness of the sheets is about 50 nm measured by atomic force microscopy (AFM) (Figure 1b). The crystalline structure of this sample was analyzed by powder X-ray diffraction. The results are shown in Figure 1c. All diffraction peaks can be indexed as monoclinic pyrrhotite-4 M Fe_7S_8 ($Fe_{1-x}S$, $x = 0.125$; JCPDS card No. 29–0723) with lattice parameters $a = 12.811$ Å, $b = 6.870$ Å, and $c = 11.885$

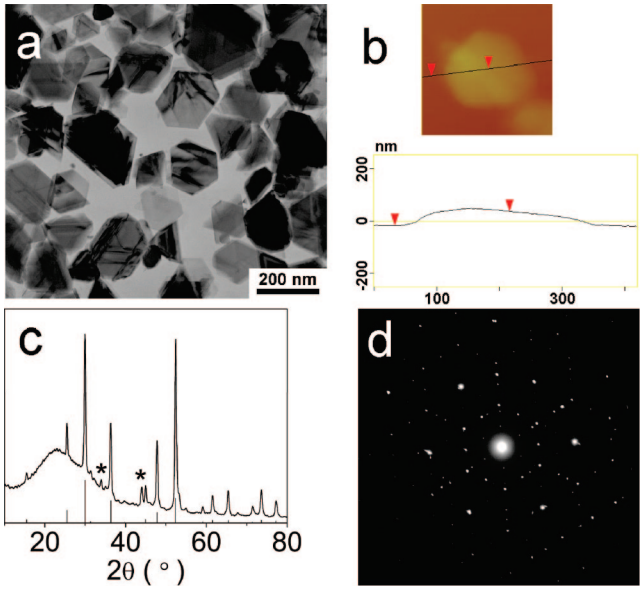

Figure 2. (a) TEM image of Fe_3S_4 nanosheets prepared at 280 °C by pyrolyzing $Fe(Ddtc)_3$ in oleylamine; (b) AFM image and the corresponding height profile of a single nanosheet; (c) XRD pattern of the nanosheets shown in panel a. The standard diffraction lines of bulk cubic gerigite Fe_3S_4 (JCPDS card 89–1998) are shown at bottom for comparison. The diffraction peaks marked with "*" corresponds to hexagonal pyrrhotite $Fe_{1-x}S$ (JCPDS card 22–1120); (d) SAED pattern of a single nanosheet.

Å. Further lattice plane analysis was performed by selected-area electron diffraction (SAED). The diffraction pattern shown in Figure 1d suggests that the top and bottom facets of Fe_7S_8 nanosheets are {001} planes.[28]

Interestingly, when the ferric complex $Fe(Ddtc)_3$ was used instead of $Fe(Ddtc)_2(Phen)$, Fe_3S_4, an analogue of magnetite with ferrimagnetic inverse thiospinel of iron,[28] was obtained. In general, the resultant Fe_3S_4 particles also present sheet structures with opposite side distance of 90–240 nm, as shown in Figure 2a. Even though the Fe_3S_4 nanosheets are smaller than the Fe_7S_8 nanosheets, their average thicknesses are nearly identical (Figure 2b). The XRD results shown in Figure 2c demonstrate that the resultant sample is mainly of cubic Fe_3S_4 (JCPDS card 89–1998; a = 9.876 Å) with impurities of hexagonal pyrrhotite $Fe_{1-x}S$ (JCPDS card No. 22–1120; a = 6.88 Å, c = 22.9 Å). Further lattice plane analysis by SAED reveal that the two hexagonal faces of each individual nanoplate are {111} crystallographic planes.[28]

Discussion

It is well-known that iron sulfide minerals are featured with significant temperature-induced composition- and phase-transformations.[8] To investigate the effects of reaction temperature on the shape, crystalline structure and chemical composition of the final products, four additional samples were prepared at 240, 260, 300, and 320 °C, respectively, using $Fe(Ddtc)_2(Phen)$ as precursor. For comparison, the reaction temperatures were equally set to 5 min.

Figure 3 presents TEM images of the iron sulfide samples obtained at 240, 260, 300, and 320 °C, respectively. It is quite obvious that the sample obtained at 240 °C also presents a quasi two-dimensional structure, but with irregular shapes. The hexagonal nanosheets start to appear in the sample prepared at 260 °C. Higher temperature generally favors the clearance of small irregularly shaped structures. However, no evident effects on the size of the nanosheets were practically observed.

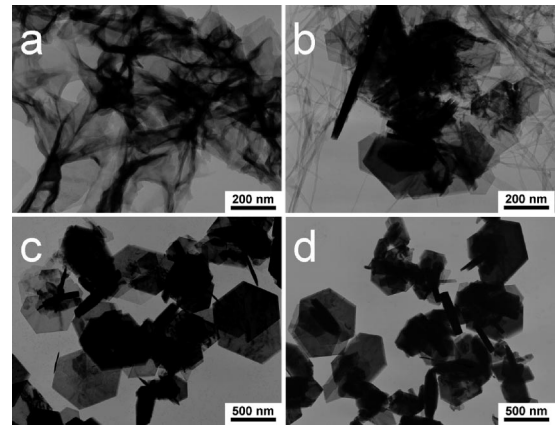

Figure 3. TEM images of iron sulfide samples synthesized at (a) 240, (b) 260, (c) 300, and (d) 320 °C, respectively, by pyrolyzing $Fe(Ddtc)_2(Phen)$ in oleylamine.

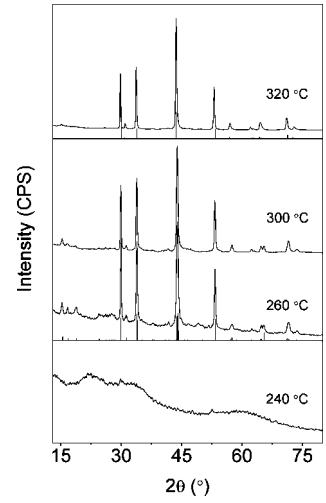

Figure 4. XRD patterns of iron sulfide samples shown in Figure 3. The standard diffraction lines of bulk hexagonal troilite FeS (JCPDS card 75–0602) and bulk monoclinic Fe_7S_8 (JCPDS card 29–0723) are given at the bottom of the upper frame and middle frame, respectively.

The XRD results shown in Figure 4 reveal that the sample prepared at 240 °C has an amorphous structure, whereas the samples obtained at 260, 300, and 320 °C, respectively, exhibit well-defined crystalline structure. More careful comparison reveals that the increase in reaction temperature led to a structural transformation in the current samples. For example, the sample prepared at 260 °C can be identified as monoclinic Fe_7S_8, whereas the sample obtained at 320 °C exhibits diffraction features of hexagonal troilite FeS (JCPDS card 75–0602; a = 3.430 Å, c = 5.790 Å). The diffraction peaks from 14 to 20° (2θ) for monoclinic Fe_7S_8 disappear. Moreover, the strongest diffraction peak also slightly shifts to low angle direction. All these changes suggest that in the current inspected reaction temperature range, high reaction temperature favors the formation of FeS, whereas low reaction temperature favors the formation Fe_7S_8. Such temperature-induced phase- and composition-transformation has been observed in bulk iron sulfide minerals, and is usually named as the first-order phase transformation (β-transition).[8,9,30]

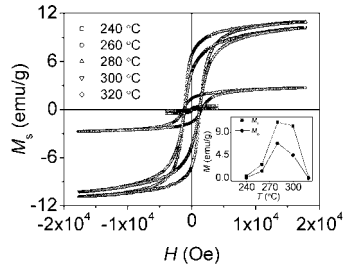

Figure 5. Hysteresis loops of iron sulfide samples synthesized at different temperatures upon the pyrolysis of $Fe(Ddtc)_2(Phen)$ in oleylamine. The measurements were carried out at room temperature. The saturation magnetization (M_s) and the remanent magnetization (M_{rs}) plotted against reaction temperature are shown in the inset.

In accompany with this transformation, the magnetic properties drastically change as shown in Figure 5. The sample prepared at 240 °C presents weak ferrimagnetic properties. With the increase in reaction temperature, the resultant samples present nonmonotonic behaviors with respect to both saturation magnetization (M_s) and the remanent magnetization (M_{rs}) as shown in the inset of Figure 5. As demonstrated by XRD, the amorphous structure is dominant in the sample prepared at 240 °C, which interprets the weak ferrimagnetic properties. As the reaction temperature increases, the crystallinity of pyrrhotite increases, undoubtedfully leading to the enhancements in both M_s and M_{rs}. In principle, Fe_7S_8 can be perceived as a derivative from ideal hexagonal FeS by extracting one iron atom per eight FeS units.[31] Consequently, the magnetic moment is generated because of reduced symmetry.[32,33] Therefore, the structural transformation from monoclinic Fe_7S_8 to hexagonal FeS inevitably leads to the decreases in both M_s and M_{rs} as the hexagonal FeS is antiferromagentic. From the magnetization measurements, it can be concluded that the phase transformation from monoclinic $Fe_7S_8$to troilite FeS occurs at above 280 °C or starts at 300 °C, which is slightly lower than that for bulk materials (315 °C),[31] probably induced by the shortened c axis in Fe_7S_8 nanosheets. Under optimized reaction temperature of 280 °C, the saturation magnetization of the resultant Fe_7S_8 nanosheets is higher than that for Fe_7S_8 nanowires reported by ref 13. This is could be a direct result of the single-crystalline structure of the current nanosheets.

The effects of reaction temperature was also investigated with respect to Fe_3S_4 nanosheets obtained using $Fe(Ddtc)_3$ precursor instead of $Fe(Ddtc)_2(Phen)$. Four additional samples apart from that shown in Figure 2 were prepared at 240, 260, 300, and 320 °C, respectively. The reaction time was also set to 5 min. The general morphologies of these four samples were characterized by TEM; the results are shown in Figure 6. Different from the sample prepared at 240 °C using $Fe(Ddtc)_2(Phen)$ (Figure 3a), the pyrolysis of $Fe(Ddtc)_3$ at the same temperature generated mainly hexagonal nanosheets as shown in Figure 6a. The general morphology remains until the reaction temperature reaches 320 °C.

More information on the phase transformation of the Fe_3S_4 samples was obtained by XRD. In general, as shown in Figure 7, the samples prepared below 300 °C present a rather similar crystalline structure, tremendously different from that obtained at 320 °C. The latter can well be assigned to pure hexagonal Fe_7S_8 (JCPDS card 24–0220; $a = 6.867$ Å, $c = 17.062$ Å). In addition, a small quantity of hexagonal $Fe_{1-x}S$ (nonstoichiometric pyrrhotite compound) is also found in the products prepared below 300 °C, which is probably caused by redox reaction between ferric ion and sulfide ion during the formation

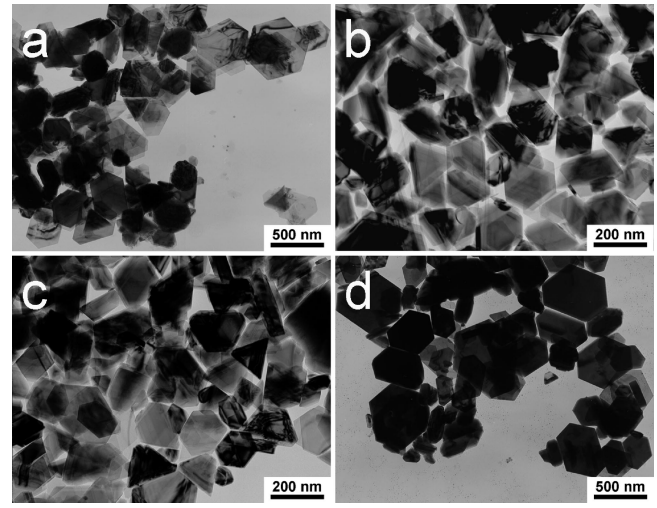

Figure 6. TEM images of iron sulfide samples synthesized at (a) 240, (b) 260, (c) 300, and (d) 320 °C, respectively, by pyrolyzing $Fe(Ddtc)_3$ in pure oleylamine.

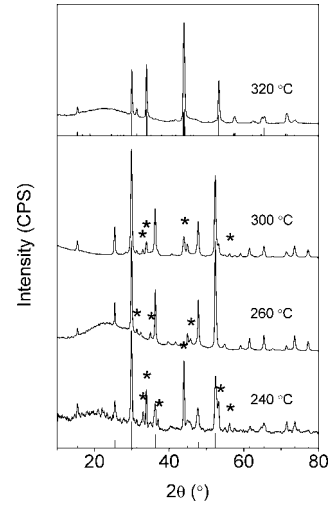

Figure 7. XRD patterns of iron sulfide samples shown in Figure 6. The standard diffraction lines of bulk hexagonal Fe_7S_8 (JCPDS card 24–0220) and bulk cubic Fe_3S_4 (JCPDS card 89–1998) are given at the bottom of the upper frame and lower frame, respectively. The diffraction peaks marked with "*" corresponds to hexagonal pyrrhotite $Fe_{1-x}S$ (JCPDS card 22–1120).

of the nanosheets, as the former has very strong reducibility, whereas the latter has mild oxidizability. Apart from the temperature-dependent chemical composition, the crystalline structure of the current series of samples also undergoes a transformation from cubic greigite to hexagonal pyrrhotite. This transformation is probably caused by the atomic rearrangement of Fe and S in the temperature range from 300 to 320 °C. Along with this transformation, even though no dramatic change in the shape of the resultant nanosheets is observed, their magnetic properties, however, change accordingly as shown in Figure 8. In general, both M_s and M_{rs}, presenting nonmonotonic behaviors against reaction temperature, reach maxima at around 280 °C and then drastically decrease against further increase of the reaction temperature due to the formation of Fe_7S_8. However, the nanosheets prepared at the same reaction temperature using $Fe(Ddtc)_2(Phen)$ as precursor were mainly antiferromagnetic FeS rather than ferrimagnetic Fe_7S_8, which strongly suggests the initial valence of iron in the precursors determines not only the

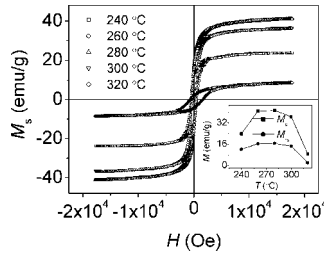

Figure 8. Hysteresis loops of iron sulfide samples synthesized at different temperatures upon the pyrolysis of $Fe(Ddtc)_3$ in oleylamine. Note that the loops recorded from samples prepared at 260 and 280 °C, respectively, are too close to differentiate. The saturation magnetization (M_s) and the remanent magnetization (M_{rs}) plotted against reaction temperature are shown in the inset.

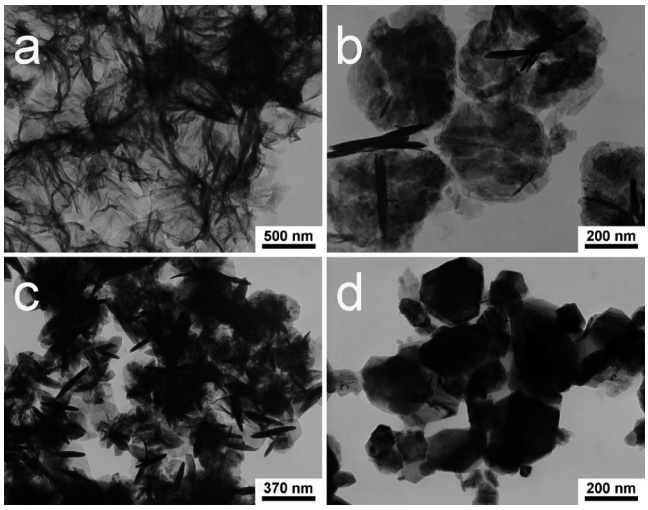

Figure 9. TEM image of samples synthesized at 280 °C by pyrolyzing $Fe(Ddtc)_2(Phen)$ in octadecence (a), or the mixture of octadecence and oleylamine (5:1) (b). The samples shown in panels c and d were obtained by prolyzing $Fe(Ddtc)_3$ in octadecence and the mixture of octadecence and oleylamine (5:1), respectively.

crystalline structure but also the chemical composition of the final nanosheets.

Apart from the reaction temperature, the reaction time is also taken as an important parameter for synthesizing nanomaterials. The influence of reaction time on the morphology of the resultant nanosheets was investigated by TEM. Unexpectedly, no obvious changes were practically observed in a time window of 5−120 min with respect to both Fe_7S_8 and Fe_3S_4 nanosheets obtained at 280 °C, suggesting that the growth of these nanosheets was thermodynamically controlled.[34] This conclusion is also supported by the fact that the naturally existing iron sulfide minerals always grow in layer structure.[12]

To elucidate the function of oleylamine ligand, additional sample were prepared for comparing with those shown in Figures 1 and 2, by replacing or partly replacing oleylamine with noncoordinating octadecene. TEM results shown in panels a and b in Figure 9 were recorded from Fe_7S_8 samples obtained by pyrolyzing $Fe(Ddtc)_2(Phen)$ in pure octadecene, and a mixture of octadecene and oleylamine (molar ratio = 5:1), respectively. The reaction temperature was 280 °C; the reaction time was set to 5 min. It is quite obvious that in both experiments, nanosheets were formed, but the latter sample presents a better defined sheet structure with round shapes. The SAED patterns on single hexagonal Fe_7S_8 nanosheet shown in Figure 1c has demonstrated that the top facet of the monoclinic

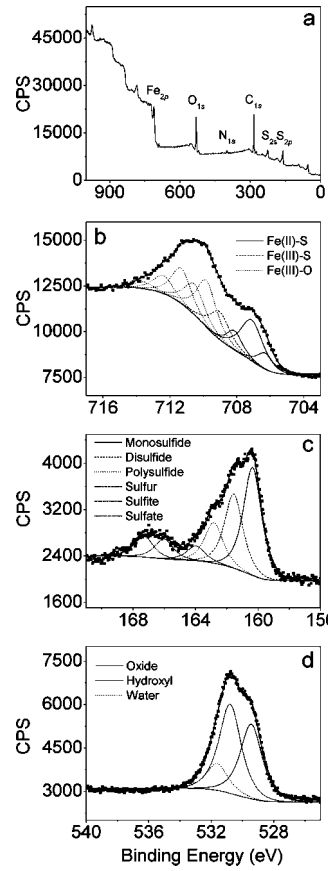

Figure 10. XPS spectra of the Fe_7S_8 hexagonal nanosheets shown in Figure 1a: (a) a survey spectrum; (b) Fe ($2p_{3/2}$) spectrum; (c) S (2p) spectrum; and (d) O (1s) spectrum, together with their corresponding fits. The measurements were carried out two days after the sample was prepared.

Fe_7S_8 nanosheets is {001} plane. Therefore, the other two facets perpendicular to {001} can be assigned to {100} and {110} planes. The shape transformation for the Fe_7S_8 nanosheets from round or quasi-hexagonal shapes to hexagonal shape found in pure oleylamine (Figure 1a) can be attributed to the effect of oleylamine ligand which controls the growth of the nanosheets along both <100> and <110> directions. Such ligand-induced facet growth is also supported by the following experiment in which the solvent was switched to a mixture of octadecene and phenylamine with a molar ratio of 5:1. In the presence of phenylamine, elongated hexagons and even parallelogrammically shaped nanosheets were obtained (see the Supporting Information), which strongly suggests that the amine group from the ligands can balance the growths of {100} and {110} facets. In contrast, the results on Fe_3S_4 demonstrated that hexagonally shaped Fe_3S_4 nanosheets can be obtained even in the absence of oleylamine as shown in Figure 9c, but the presence of oleylamine helps to prevent the hexagonal nanosheets from agglomerating (Figure 9d), on the other hand, giving rise to more regularly shaped nanosheets as shown in Figure 2a.

In fact, most naturally existing iron sulfide minerals are metastable under the ambient atmosphere.[10] Therefore, the air stabilities of the resultant Fe_7S_8 and Fe_3S_4 nanosheets, shown in both Figures 1a and 2a were investigated by XPS. The first round of measurements was performed 2 days after the preparations. The XPS results recorded from the Fe_7S_8 sample are shown in Figure 10. The emission shoulder shown in Figure 10b at low energy side can be attributed to Fe(II) ion forming an Fe(II)−S bond, whereas the emission peak at high energy

Table 1. Best Fitting Data for Fe ($2p_{3/2}$), S (2p), and O (1s) Signals Recorded from the Fe_7S_8 Hexagonal Nanosheets after They Were Exposed to Air for 2 Days

B.E. (eV)	fwhm	area (%)	chemical state
		Fe ($2p_{3/2}$)	
707.0	1.1	5.2	Fe(II)-S[b]
707.8	1.6	19.5	Fe(II)-S[a]
708.8	1.1	6.3	Fe(II)-S[b]
709.7	1.4	11.6	Fe(III)-S[a]
710.5	1.4	19.4	Fe(III)-O[a]
711.2	1.4	12.9	Fe(III)-O[b]
712.0	1.4	14.7	Fe(III)-O[b]
713.1	1.4	7.6	Fe(III)-O[b]
714.3	1.4	2.8	Fe(III)-O[b]
		S (2p)	
161.0	1.38	38.6	S^{2-}
162.2	1.38	26.6	S_2^{2-}
163.5	1.38	14.5	S_n^{2-}
164.6	1.38	5.3	S
166.7	1.38	7.1	SO_3^{2-}
168.0	1.38	7.9	SO_4^{2-}
		O (1s)	
530.1	1.66	39.1	O^{2-}
531.5	1.66	46.9	$OH^-/SO_3^{2-}/SO_4^{2-}$
532.3	1.66	14.0	H_2O

[a] Major peak. [b] Multiplet.

Table 2. Experimental Results on Atomic Ratios Among Fe, O, and S in the Fe_7S_8 Nanosheets after Being Exposed to Air for Different Time Periods

	O:Fe	S:Fe
2 days	2.61	1.18
5 months	2.94	1.25

side can roughly be assigned to Fe(III) bonded with S and O.[35,36] The binding energy of Fe ($2p_{3/2}$) was carefully fitted. The best fits are tabulated in Table 1. The major peak of Fe(II) was found to be located at 707.8 eV with two multiplets occurring about 1.0 eV above and 0.8 eV below the major peak. The major peak of Fe(III) bonded with O is located at 710.5 eV with four multiplets peaking at 711.2, 712.0, 713.1 and 714.3 eV, respectively, while the last peak locating at 709.7 eV can be assigned to the major peak of Fe(III) bonded with S. In principle, all these assignments are in good agreement with the reference results.[35] The only discrepancy is that the multiplets around the major Fe(III)−S peak are missing.[35,36] Nonetheless, the ratio of Fe(II):Fe(III) derived from the fitting results, 2.67, is just slightly higher than the theoretical value of 2.50 for Fe_7S_8, suggesting that the fitting results for Fe are reasonable. More supports were given by the analysis of S (2p) signal shown in Figure 10c. The results in Table 1 suggest that 6 types of sulfur-containing species coexist in the current sample, i.e., monosulfide, disulfide, polysulfides, sulfur, sulfite, and sulfate species.[35–37] Among them, monosulfide contributes 38.6% of the total S (2p) signal, whereas the Fe signal analysis reveals that the contents of Fe(III) and Fe(II) bonded with S are 11.6 and 31.0%, respectively. Therefore, the overall elemental ratio between S and Fe in the investigated sample is calculated to be around 1.25:1 (= (11.6%(Fe(III) × (3/2) + 31.0%Fe(II))/38.6%(S^{2-})), which is rather close to the experimental result of 1.18 shown in Table 2. It can thus be concluded that the above fittings are generally reliable.

The fitting results for O (1s) spectrum in Figure 10d reveal that oxygen mainly exists in the form of oxides, hydroxyl groups, and adsorbed water in the Fe_7S_8 sample.[35–37] Because the binding energies of O (1s) in S−O and Fe−OH bonds are very close,[38] the amount of OH can only be extracted from data

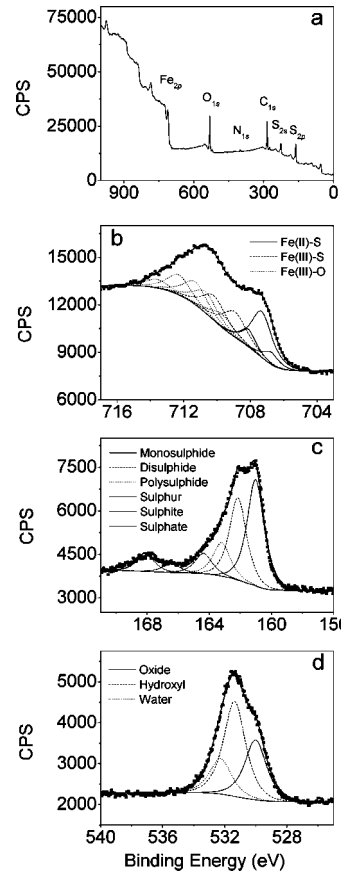

Figure 11. XPS spectra of the Fe_3S_4 hexagonal nanosheets shown in Figure 2a: (a) a survey spectrum; (b) Fe ($2p3/2$) spectrum; (c) S (2p) spectrum; and (d) O (1s) spectrum, together with their corresponding fits. The measurements were carried out two days after the sample was prepared for $Fe(OH)_3$. Therefore, it can be concluded that the oxidation products of Fe_7S_8 are mainly amorphous $Fe(OH)_3$ and FeOOH.

obtained from the XPS analysis on S, i.e., 22.5% of total O atoms existing in OH form, whereas 39.1% of total O atoms occur in oxides. As the overall O:Fe ratio is 2.61:1 and 57.4% of Fe atoms are bonded with O, the ratio between Fe and O in the species containing Fe(III)−O bonds is therefore estimated to be 2.78:1, quite approaching the stoichiometric value for $Fe(OH)_3$. Therefore, it can be concluded that the oxidation products of Fe_7S_8 are mainly amorphous $Fe(OH)_3$ and FeOOH.

To further evaluate the air stabilities of nanosheets, the XPS measurements were repeated five months later. The experimental results on the O:Fe and S:Fe ratios are given in the second row of Table 2. By similar analytical procedures mentioned above, Fe ($2p_{2/3}$), S (2p) and O (1s) spectra were fitted and the results are provided in Supporting Information. In comparison with the 2-day old sample, the 5-month old sample simply presents a slightly higher degree of oxidation, suggesting that the oxidation of Fe_7S_8 nanosheets was nearly completed within the first 48 h after the preparation, which is consistent with the literature results.[35]

With respect to Fe_3S_4 nanosheets, the XPS results from the first round of measurements are shown in Figure 11. The best fits on Fe ($2p_{3/2}$) signal, presented in Figure 11b as well as Table 3, reveal that there exist Fe(II) bonded with S and Fe(III) bonded with both S and O.[37,39] Nevertheless, all binding energies for Fe(II)−S, Fe(III)−S, and Fe(III)−O are in general shifts to lower energy side in comparison with those for Fe_7S_8 sample for several tenths eV, which might be caused by calibration. Similar to Fe_7S_8, Fe_3S_4 sample also presents one peak at 709.0 eV for

Table 3. The best fitting results for Fe ($2p_{3/2}$), S ($2p$), and O ($1s$) spectra recorded from the Fe_3S_4 hexagonal nanosheets after they were exposed to air for two days

B.E. (eV)	fwhm	area (%)	chemical state
		Fe ($2p_{3/2}$)	
706.8	1.1	4.8	Fe(II)-S[b]
707.4	1.6	22.2	Fe(II)-S[a]
708.2	1.1	5.5	Fe(II)-S[b]
709.0	1.6	13.0	Fe(III)-S[a]
710.0	1.6	15.1	Fe(III)-O[a]
710.7	1.6	13.8	Fe(III)-O[b]
711.4	1.6	11.4	Fe(III)-O[b]
712.3	1.6	9.8	Fe(III)-O[b]
713.6	1.6	4.4	Fe(III)-O[b]
		S (2p)	
161.1	1.3	39.3	S^{2-}
162.2	1.3	30.5	S_2^{2-}
163.2	1.3	12.5	S_n^{2-}
164.4	1.3	7.6	S
166.5	1.3	3.4	SO_3^{2-}
168.1	1.3	6.8	SO_4^{2-}
		O (1s)	
530.1	1.66	31.5	O^{2-}
531.5	1.66	49.9	$OH^-/SO_3^{2-}/SO_4^{2-}$
532.3	1.66	18.6	H_2O

[a] Major peak. [b] Multiplet.

Table 4. Experimental Results on Atomic Ratios Among Fe, O, and S in the Fe_3S_4 Nanosheets after Being Exposed to Air for Different Time Periods

	O:Fe	S:Fe
2 days	2.74	1.03
5 months	4.63	2.14

Fe(III) bonded with S without showing any multiplets. However, further calculations as performed for Fe_7S_8 also confirms the reliability of the fits for Fe, by taking the data of S (2p), O (1s) (Table 3) as well as the overall elemental ratio among Fe, O, and S (Table 4.) into considerations. From the fitting results shown in Table 3, it can be found out that the Fe(II)−S content (32.5%) does not alter much in comparison with the stoichiometric value (33.3%) for Fe(II) in Fe_3S_4. In contrast, the Fe(III)−S content drops drastically from the theoretical value of 66.7 to 11.9%, implying that the oxidation reaction in Fe_3S_4 nanosheets starts favorably from the Fe(III)−S bonds.

Tremendously different from Fe_7S_8, 5 month air-exposure led to severe oxidation to Fe_3S_4 nanosheets. More detailed results provided in Supporting Information demonstrate that only 4.6% Fe(II)−S and 7.0% Fe(III)−S eventually remained 5 months later, demonstrating that the greigite nanosheets have much worse air stability than pyrrhotite nanosheets over long-term of exposure to air. Moreover, the long-term oxidation favors a greater decrease in Fe(II)−S content. In the mean time, with the disappearance of sulfate species and the decrease of monosulfide species, the contents of disulfide, polysulfide sulfur, and sulfite species increase, which suggests that redox reaction between the monosulfide and sulfate species occurred during sample storage.

On the basis of the overall XPS analysis, the following conclusions can be arrived at: (1) Fe(III)−S bond triggers the oxidation in both Fe_7S_8 and Fe_3S_4 nanosheets, which is supported by facts that the Fe(III)−S contents in both samples decrease faster in earlier days than those for Fe(II)−S. Therefore, higher Fe(III)−S content is unfavorable for the air stability of iron sulfides. (2) Water and oxygen are involved in the oxidation reactions for both Fe_7S_8 and Fe_3S_4 nanosheets. (3) The oxidation of Fe(II)−S may occur via an intermediate stage of Fe(III)−S because Fe(II) oxidizes more easily than S^{2-},[40] which interprets the fact that a certain percentage of Fe(III)-S content remained even in (Fe(III)−S)-rich sample (Fe_3S_4) after long-term oxidation rather than completely disappeared.

Summary and Conclusions

In the present work, two-dimensional magnetic pyrrhotite Fe_7S_8 and greigite Fe_3S_4 nanosheets are synthesized by pyrolyzing $Fe(Ddtc)_2(Phen)$ and $Fe(Ddtc)_3$ in oleylamine, respectively. Because both sulfur and iron coexist in each complex, the synthetic route of single source precursor is consequently enabled. The chemical compositions of the resultant iron sulfide nanosheets are found to be determined by the initial valances of iron in precursors. Typically, ferrous complex leads to Fe_7S_8 nanosheets while ferric complex gives rise to Fe_3S_4 nanosheets. Under optimized reaction temperature of 280 °C, highly crystallized Fe_7S_8 and Fe_3S_4 nanosheets obtained mainly exist in hexagonal shape. Moreover, the reaction temperature also plays a critical role in controlling the chemical compositions, morphologies, crystalline structures and even the magnetic properties of the resultant iron sulfide nanosheets. Further experimental results based on different types of solvents suggest that the formation of nanosheet structures is thermodynamically controlled, whereas the formation of hexagonally shaped Fe_7S_8 nanosheets is probably kinetically controlled as amine group from the surface ligands are required. In contrast, hexagonal Fe_3S_4 nanosheets can be obtained even in the absence of oleylamine. Nevertheless, oleylamine has been demonstrated to be necessary for preventing the resultant nanosheets from agglomerating. Systematic XPS investigations reveal that the above-mentioned hexagonal nanosheets are not stable in ambient conditions. Because the oxidation is triggered by Fe(III)−S in the system, Fe_3S_4 presents even a worse air-stability over long time of storage. Even though the coexistence of strongly reducible ferric ion and mildly oxidizable sulfide ion in Fe_3S_4 and Fe_7S_8 makes their composition controls rather difficult, the current investigations has provided a relatively reliable single-precursor route for preparing stoichiometrical iron sulfides nanosheets, which could be valuable for further investigating the preparations of nanosized iron sulfides with well-defined crystalline structures, compositions, and morphologies.

Acknowledgment. Funding was jointly provided by NSFC projects (20673128, 20640430564).

Supporting Information Available: FTIR spectra and data lists of complexes $Fe(Ddtc)_2(Phen)$ and $Fe(Ddtc)_3$, TEM images of Fe_7S_8 and Fe_3S_4, XPS spectra, and fitting data lists of Fe_7S_8 and Fe_3S_4 nanosheets (PDF). This information is available free of charge via the Internet at http://pubs.acs.org.

References

(1) Zeng, H.; Li, J.; Liu, J. P.; Wang, Z. L.; Sun, S. H. *Nature* **2002**, *420*, 395.
(2) Bulte, J. W. M.; Douglas, T.; Witwer, B.; Zhang, S. C.; Strable, E.; Lewis, B. K.; Zywicke, H.; Miller, B.; Gelderen, P. V.; Moskowitz, B. M.; Duncan, L. D.; Frank, J. A. *Nat. Biotechnol.* **2001**, *19*, 1141.
(3) Nam, J. M.; Thaxton, C. S.; Mirkin, C. A. *Science* **2003**, *301*, 1884.
(4) Jordan, A.; Scholz, R.; Maier-Hauff, K.; Johannsen, M.; Wust, P.; Nadobny, J.; Schirra, H.; Schmidt, H.; Deger, S.; Loening, S.; Lanksch, W.; Felix, R. *J. Magn. Magn. Mater.* **2001**, *225*, 118.
(5) Hu, F.; Wei, L.; Zhou, Z.; Ran, Y.; Li, Z.; Gao, M. *Adv. Mater.* **2006**, *18*, 2553.
(6) Li, Z.; Wei, L.; Gao, M.; Lei, H. *Adv. Mater.* **2005**, *17*, 1001.

(7) Huh, Y.-M.; Jun, Y.; Song, H.-T.; Kim, S.; Choi, J.; Lee, J.-H.; Yoon, S.; Kim, K.-S.; Shin, J.-S.; Suh, J.-S.; Cheon, J. *J. Am. Chem. Soc.* **2005**, *127*, 12387.
(8) Rao, C. N. R.; Pisharody, K. P. R. *Prog. Solid State Chem.* **1976**, *10*, 207.
(9) Ward, J. C. *Rev. Pure Appl. Chem.* **1970**, *20*, 175.
(10) Rickard, D.; Luther, III, G. W. *Chem. Rev* **2007**, *107*, 514.
(11) Makovicky, E. *Rev. Mineral Geochem.* **2006**, *61*, 7.
(12) Vaughan, D. J.; Craig, J. R. *Mineral Chemistry of Metal Sulfides*; Cambridge University Press: Cambridge, U.K., 1978.
(13) Nath, M.; Choudhury, A.; Kundu, A.; Rao, C. N. R. *Adv. Mater.* **2003**, *15*, 2098.
(14) He, Z.; Yu, S-H.; Zhou, X.; Li, X.; Qu, J. *Adv. Funct. Mater.* **2006**, *16*, 1105.
(15) Chen, X.; Wang, Z.; Wang, X.; Wan, J.; Liu, J.; Qian, Y. *Inorg. Chem.* **2005**, *44*, 951.
(16) Kong, X.; Lou, T.; Li, Y. *J. Alloys Compd.* **2005**, *390*, 236.
(17) Shi, X.; Sun, K.; Balogh, L.; Baker, J. R., Jr *Nanotechnology* **2006**, *17*, 4554.
(18) Burda, C.; Chen, X.; Narayanan, R.; El-Sayed, M. A. *Chem. Rev.* **2005**, *105*, 1025.
(19) Park, J.; An, K.; Hwang, Y.; Park, J. G.; Noh, H. -J.; Kim, J. Y.; Park, J. H.; Hwang, N. M.; Hyeon, T. *Nat. Mater.* **2004**, *3*, 891.
(20) Cheon, J.; Kang, N. J.; Lee, S. M.; Lee, J. H.; Yoon, J. -H.; Oh, S. J. J. *Am. Chem. Soc.* **2004**, *126*, 1950.
(21) Liu, X. M; Fu, S. -Y.; Xiao, H. M. *Mater. Lett.* **2006**, *60*, 2979.
(22) Wang, J.; Chen, Q.; Hou, B.; Peng, Z. *Eur. J. Inorg. Chem.* **2004**, 1165.
(23) Lee, K. B.; Park, S.; Mirkin, C. A. *Angew. Chem., Int. Ed.* **2004**, *43*, 3048.
(24) Cao, M.; Liu, T.; Gao, S.; Sun, G.; Wu, X.; Hu, C.; Wang, Z. L. *Angew. Chem., Int. Ed.* **2005**, *44*, 4197.
(25) Zou, G.; Xiong, K.; Jiang, C.; Li, H.; Wang, Y.; Zhang, S.; Qian, Y. *Nanotechnology* **2005**, *16*, 1584.
(26) Zhao, F.; Sun, H. L.; Su, G.; Gao, S. *Small* **2006**, *2*, 244.
(27) Mirkovic, T.; Hines, M. A.; Nair, P. S.; Scholes, G. D. *Chem. Mater.* **2005**, *17*, 3451.
(28) Wang, Z. L. *J. Phys. Chem. B* **2000**, *104*, 1153.
(29) Skinner, B. J.; Erd, R. C.; Grimaldi, R. F. *Am. Mineral.* **1964**, *49*, 543.
(30) Li, F.; Franzen, H. F. *J. Alloys Compd.* **1994**, *215*, L3.
(31) Wang, H.; Salveson, I. *Phase Transitions* **2005**, *78*, 547.
(32) Wang, H.; Pring, A.; Wu, F.; Chen, G.; Jiang, J.; Xia, F.; Zhang, J.; Ngothai, Y.; O'Neill, B. *J. Sulfur Chem.* **2006**, *27*, 271.
(33) Pearce, C. I.; Pattrick, R. A. D.; Vaughan, D. J. *Rev. Mineral Geochem.* **2006**, *61*, 127.
(34) Xiong, Y,; McLellan, J. M.; Chen, J.; Yin, Y.; Li, Z. Y.; Xia, Y. *J. Am. Chem. Soc.* **2005**, *127*, 17118.
(35) Pratt, A. R.; Muir, I. J.; Nesbitt, H. W. *Geochim. Cosmochim. Ac.* **1994**, *58*, 827.
(36) Mycroft, J. R.; Nesbitt, H. W.; Pratt, A. R. *Geochim. Cosmochim. Acta* **1995**, *59*, 721.
(37) Boursiquot, S.; Mullet, M.; Abdelmoula, M.; Génin, J.-M.; Ehrhardt, J.-J. *Phys. Chem. Miner.* **2001**, *28*, 600.
(38) http://srdata.nist.gov/xps/Bind_E.asp.
(39) Herbert Jr, R. B.; Benner, S. G.; Pratt, A. R.; Blowes, D. W. *Chem. Geol.* **1998**, *144*, 87.
(40) The standard redox potentials for Fe^{2+}/Fe^{3+} and S^{2-}/S pairs are– 0.771 and 0.407 V, respectively. See *Lange's Handbook of Chemistry*, 16th ed.; Speight, J. G., Ed.; McGraw-Hill: New York, 2005.

CG701075U